Roles of Octabutoxy Substitution and J-Aggregation in Stabilization of the Excited State in Nickel Phthalocyanine

ARTICLE *in* THE JOURNAL OF PHYSICAL CHEMISTRY A · JUNE 2014

Impact Factor: 2.69 · DOI: 10.1021/jp5036629 · Source: PubMed

5 AUTHORS, INCLUDING:

Petr Toman
Academy of Sciences of the Czech Republic
91 PUBLICATIONS **637** CITATIONS
SEE PROFILE

Miroslav Menšík
Academy of Sciences of the Czech Republic
32 PUBLICATIONS **41** CITATIONS
SEE PROFILE

Jiri Pfleger
Academy of Sciences of the Czech Republic
73 PUBLICATIONS **806** CITATIONS
SEE PROFILE

THE JOURNAL OF PHYSICAL CHEMISTRY A

Article

pubs.acs.org/JPCA

Roles of Octabutoxy Substitution and J-Aggregation in Stabilization of the Excited State in Nickel Phthalocyanine

David Rais,[†] Petr Toman,[†] Jiří Černý,[‡] Miroslav Menšík,[†] and Jiří Pfleger*[,†]

[†]Institute of Macromolecular Chemistry, Academy of Sciences of the Czech Republic, v. v. i., Heyrovského nám. 2, 162 06 Prague, Czech Republic

[‡]Centre for Organic Chemistry Ltd., Rybitví 296, 533 54 Rybitví, Czech Republic

Supporting Information

ABSTRACT: Nickel phthalocyanine (NiPc) complexes are known to show a rapid nonradiative deactivation of the photoexcited state through the internal conversion. This could be exploited in practical applications, such as photoprotection and photodynamic therapy. The butoxy substitution of NiPc plays an important role for drug delivery but also greatly influences its photophysics. We prepared novel peripherally substituted 2,3,9,10,16,17,23,24-octabutoxy nickel(II) phthalocyanine and characterized the deactivation pathway of its photoexcited state in solution by femtosecond transient absorption spectroscopy and quantum chemical calculations. We bring experimental evidence for the kinetic model, in which the photoexcitation evolves in two independent branches. In the first branch, assigned to the monomer, it undergoes ultrafast intersystem crossing to a triplet state, which subsequently decays to the ground state through a pathway involving lower-lying triplet states, with a ground-state recovery lifetime of 814 ps. It is about three-times longer than the lifetime published for unsubstituted NiPc. In the second branch, the photoexcitation decayed to a triplet state with an orders of magnitude longer lifetime, with the quantum yield of about 4%. This state showed spectral features of J-aggregates. These findings are important for the applications that rely on singlet oxygen formation or fast nonradiative deactivation of the excited state.

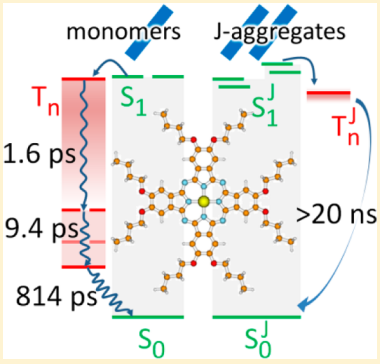

INTRODUCTION

Derivatives of phthalocyanine (Pc) are known as important dye molecules, with a strong potential for practical application in many fields of industry due to their large extinction coefficient, optical absorption extended to the near-infrared spectral region, and a very good photochemical stability, one of the best known among synthetic organic materials.[1] Among them, the nickel phthalocyanine (NiPc) complexes are known for their rapid nonradiative deactivation of the photoexcited state through an internal conversion.[2−4]

Recently, Fournier et al. reported[5] on the excited-state evolution in NiPc sulfonate and mentioned it as a potentially effective photodynamic therapy sensitizer acting on the basis of photothermal effects, which does not require the presence of molecular oxygen for killing cancer tissue cells.[6] In another Pc derivative bearing octabutoxy substituents, the liposome-mediated targeting allowed the delivery of a photosensitizer into a tumor tissue and also accelerated its subsequent clearance compared to sensitizers substituted with nonpolar groups.[7] The fast nonradiative excited-state deactivation was used to kill cancer cells in vivo by photoinduced localized heating of the tissue using a high concentration of the dye.

In the first report on ultrafast nonlinear transient optical absorption behavior of NiPc (nonsubstituted),[8] the authors found that the initially created photoexcited state S_1 relaxes with time constant (2.8 ± 0.2) ps into a manifold of nonabsorbing excited states of higher spin multiplicity, located in energy below S_1. However, they did not study subsequent evolution of the excited state. The photophysics of crown-ether-substituted NiPc was studied in detail with pump−probe transient absorption (TA) spectroscopy by Nikolaitchik and Rodgers.[3] They found that the photoexcited S_1 state undergoes ultrafast intersystem crossing (ISC) to a vibrationally hot triplet state with the electron density localized at the central metal atom within the time resolution of their instrumentation. It is known from the cited work that the unfilled d orbitals of Ni(II) interact with the large π-electron system of Pc, which creates pathways for fast nonradiative excited state deactivation.

The nonperipherally octabutoxy-substituted nickel phthalocyanine (NiPc(α-O-Bu)$_8$) was thoroughly investigated both experimentally and theoretically in the work of Soldatova et al.[4] The authors presented valuable information identifying effects of octabutoxy substitution resulting in a substantial bathochromic shift of the Q band absorption (from 670 to 740 nm) and about a 2-fold increase of the ground-state repopulation lifetime (300 ps for NiPc and 640 ps for NiPc(α-O-Bu)$_8$). However, the nonperipheral octa-substitution with butoxy groups induces a combined effect of large planarity distortion (due to steric effects) together with their strong electron-donating effect.[9]

Received: April 14, 2014
Revised: June 12, 2014
Published: June 26, 2014

We present the analysis of the photophysical behavior of peripherally substituted 2,3,9,10,16,17,23,24-octabutoxy nickel(II) phthalocyanine studied by UV−vis optical absorption and time-resolved TA spectroscopy as well as density functional theory (DFT) quantum chemical calculations. By comparing it with the published results for NiPc and NiPc(α-O-Bu)$_8$, we aim to separate the electron-donating effects from the steric hindrance effects imposed on NiPc by symmetric eight-fold substitution with butoxy groups because it is expected that the peripheral substitution does not induce planarity distortion of NiPc.

MATERIALS AND METHODS

We prepared 2,3,9,10,16,17,23,24-octabutoxy nickel(II) phthalocyanine (compound **1**, cf. Figure 1) by a modification of the

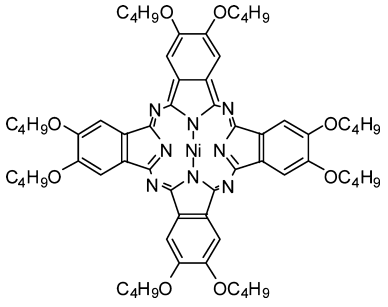

Figure 1. Chemical structure of the 2,3,9,10,16,17,23,24-octabutoxy nickel(II) phthalocyanine, compound **1**.

Wöhrle method[9] from 4,5-dibutoxyphthalonitrile. The starting nitrile was prepared according to the procedure described previously[10,11] in three steps, with an overall yield of 63% (cf. Scheme 1).

Scheme 1. Synthetic Route to the Studied Compound 1

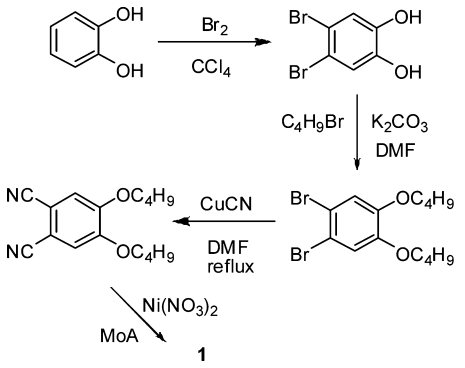

A well-ground mixture of 4,5-dibutoxyphthalonitrile (16.34 g, 60 mmol), nickel(II) nitrate hexahydrate (4.37 g, 15 mmol), ammonium molybdate (0.45 g, 0.5 mmol), and anhydrous sodium sulfate (75 g) was placed in a glass tube (on air), heated to 200 °C for 1 h, and kept for 3 h at the same temperature. Then, the resulting mixture was cooled down slowly to 25 °C, ground, and washed well with water to remove all salts. The crude product was washed with ethanol (300 mL), acetone (2 × 300 mL), and 0.02 M methanolic HCl (500 mL). Fluorescent impurity was removed in a Soxhlet apparatus using methanol. Yield: 5 g (29%), mp > 300 °C. UV−vis ($CHCl_3$, c = 27 mg/L) λ_{max} (log ε): 290 (4.91), 405 (4.45), 609 (4.43), 671 (4.92). ^{13}C NMR ($CDCl_3$), δ: 150.19; 142.43; 128.99; 102.77 (4 × C_{arom}); 68.41 (−OCH_2); 31.69; 19.55; 14.21 (3 × C_{aliph}). The compound was a green solid. It was easily soluble in $CHCl_3$, CH_2Cl_2, toluene, and pyridine and insoluble in water, ethanol, and methanol. It was not possible to analyze standard ^{1}H NMR spectra due to its strong paramagnetic properties (resulting in very broad signals), whereas the ^{13}C NMR signals were only negligibly affected by the paramagnetism.

For the photophysical measurements, the sample was further purified by flash chromatography using methanol and a methanol−chloroform gradient. The impurity was completely removed as indicated by TLC using silica gel and methanol as an eluent. The purified powder of the compound **1** was dissolved in toluene (ACS grade, Sigma-Aldrich) at the concentration 10^{-4} M. The solution was maintained at 60 °C in an ultrasonic bath for 30 min to speed up the dissolution. This stock solution was further diluted with toluene to the desired concentration for the optical absorption spectroscopy.

Steady-state UV−vis optical absorption spectra of solutions were acquired at room temperature in 10 or 1 mm quartz cuvette using a PerkinElmer Lambda 950 spectrophotometer.

Pump−probe TA spectra of the dye solutions were measured using a HELIOS spectrometer (Ultrafast Systems, LLC). The pump pulses were generated in a cascade of lasers consisting of the primary oscillator Mantis providing a seed pulse train to the regenerative amplifier Legend (Coherent, Inc.). The output was directed into the TOPAS-C (Light Conversion Ltd.) optical parametric amplifier. The system generated pump pulses with a 670 nm central wavelength at the repetition rate of 1 kHz. Every second pump pulse was selected for the sample excitation using a synchronized mechanical chopper working at the repetition rate of 500 Hz; the pulse energy was adjusted to 5.3 μJ. After the pump pulses passed through a depolarizer, they were focused on the sample using a plano-convex spherical lens. The probe pulses were derived from the output of the regenerative amplifier, passed through a delay line, and focused with a spherical mirror onto a sapphire crystal for the white-light continuum generation (400−800 nm). We used a dual beam configuration employing two identical iCCD-based array spectrometers (for the sample and reference beam, respectively, with a resolution of 1 nm per channel). The sample solutions were measured in a standard stationary quartz spectroscopic cell with a 2 mm optical path (Starna cells) under continuous stirring with a magnetic stirrer, under conditions of effectively a pseudo-single-shot experiment. Under these conditions, the sample degradation was avoided. The cell-induced group velocity dispersion over the spectrum of the broad-band probe pulse was characterized and included in the spectro-temporal model.

TA data analysis was done with help of the computer software Glotaran[12] and TIMP.[13] The software was used to develop a suitable kinetic model by means of the global analysis method[14] and to fit parameters of the model by the target analysis method.[15] The confidence intervals determined for the calculated kinetic rate constants were given at a 95% probability level. Prior to the kinetic model analysis, the TA data obtained with pure solvent were subtracted from the data acquired with the sample solution in order to reject the experimental artifacts arising from the solvent and cuvette walls.

Quantum chemical calculations were done using the Gaussian 09 program package.[16] The ground-state molecular geometry of the studied Pc derivative was determined by means of the minimization of the total energy calculated by the DFT

dx.doi.org/10.1021/jp5036629 | J. Phys. Chem. A 2014, 118, 5419−5426

method M06-L[17] using the 6-31G(d) basis set. DFT methods were selected because they proved recently to successfully calculate the conformations, vibrational frequencies, optical absorption spectra, and many other properties of various conjugated organic molecules.[18−23] The M06-L method uses a local functional, which seems to be the most accurate for transition metals, and it is the only local functional with better across-the-board average performance than the popular method B3LYP.[24] Its localization allows using highly efficient algorithms to reduce the computational cost for large molecules. To reduce energy oscillations and increase numerical accuracy during the molecular geometry optimization, two-electron integrals and their derivatives were calculated using the pruned (99,590) integration grid, having 99 radial shells and 590 angular points per shell (Gaussian 09 keyword "Int=UltraFine"). As a standard simplification used in many quantum chemical studies, the molecules were considered to be isolated during the geometry optimization. Because Pc is a very rigid molecule, this approximation causes no significant errors in the molecular geometry and substantially speeds up the calculation.

On the basis of the optimized vacuum ground-state geometry, 60 lowest singlet and 60 lowest triplet vertical excited states were computed by the time-dependent version (TD-) of the DFT method,[24−26] employing the Coulomb-attenuated hybrid exchange−correlation (CAM−B3LYP) functional[27−29] and using the 6-311+G(d) basis set. This long-range corrected functional has been found to properly predict excitation energies in optical absorption spectra.[30] In order to include solvatochromic effects, these single-point calculations were performed in the toluene solution using the polarizable continuum model (PCM).[31]

The quantum yield of singlet oxygen ($^1O_2$) photoproduction was measured using the spectrophotometric method described previously[32] with indicator 1,3-diphenylisobenzofurane, which reacts exclusively with $^1O_2$, giving 1,2-dibenzoylbenzene as a stable final product.[33] The photobleaching of the indicator was monitored at 418 nm during irradiation of the sample with laser light with λ_{max} = 661 nm. The reactions followed the first-order kinetics, and the rate constant k_Δ could be determined. In order to obtain the quantum yield of the singlet oxygen production φ_Δ, the method requires calibration measurement of the photobleaching rate k_{std} with a photosensitizer of a priori known quantum yield φ_{std}

$$\varphi_\Delta = \varphi_{std}\frac{k_\Delta}{k_{std}} \quad (1)$$

We used unsubstituted zinc(II) phthalocyanine with φ_{std} = 0.58.[32,34] The concentration of the toluene solution of the compound **1** was 1 mg/L.

RESULTS AND DISCUSSION

The UV−vis optical absorption spectra of the toluene solution of **1** presented in Figure 2 for various concentrations show the same features as the UV−vis spectra of previously published analogues.[4,35,36] For the lowest concentration ($c = 10^{-6}$ M), we observed two groups of absorption bands. On the red side of the spectrum, there is a Q band[37] with three distinct maxima at 670, 641, and 604 nm, denoted as Q_{00}, Q_{01}, and $Q_{01'}$, respectively, to highlight their vibrational origin arising from different modes.[37] On the UV side of the spectra, we observed a broad B band absorption.[37] On the basis of our DFT quantum

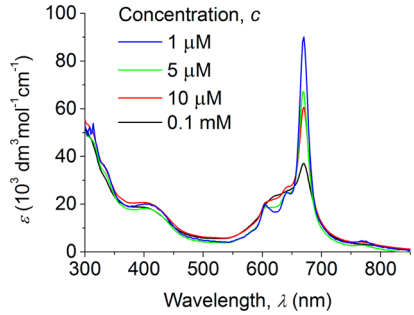

Figure 2. Molar extinction coefficient spectra $\varepsilon(\lambda)$ of **1** in toluene for various concentrations.

chemical calculations, we could assign the experimentally observed absorption peak Q_{00} to the transition between the multielectron singlet ground state S_0 (symmetry $^1A_{1g}$) and the double-degenerate singlet state (^1E_u symmetry, with calculated energy $h\nu_{DFT}$ = 1.91 eV, transition HOMO → LUMO, LUMO +1, and first excited state S_1) with good agreement. There was only a 61 meV difference between the calculated and experimentally determined positions of Q_{00} ($h\nu_{exp}$ = 1.85 eV, cf. Figure S1 (Supporting Information) and Table 1).

Table 1. Vertical Transition Energy, $h\nu_{DFT}$, Excited-State Symmetry, and Oscillator Strength, f_{DFT}, of Selected Electronic Transitions from the $^1A_{1g}$ Ground State Calculated by the DFT Method and Assignment to the Decay Times of the Particular Exited States Observed in the TA Spectra

trans. No.:	symmetry	$h\nu_{DFT}$ (eV)	λ_{DFT} (nm)	f_{DFT}[a]	τ_i (ps), notes
all spin-forbidden transitions energetically below S_1:					
1	$^3B_{1g}$	0.416	2984	0	
2	^3E_u	0.584	2122	0	(814 ± 25)
3	^3E_u	0.584	2122	0	(9.4 ± 0.5)
4	^3E_g	0.861	1441	0	
5	^3E_g	0.861	1441	0	
6	$^3A_{2g}$	2.086	594	0	(1.60 ± 0.04)
lowest spin-allowed, symmetry-allowed transitions:					
1	^1E_u	1.912	648	0.674	HOMO → LUMO, LUMO+1
2	^1E_u	1.912	648	0.675	
10	^1E_u	3.312	374	0.079	
11	^1E_u	3.312	374	0.079	HOMO-4, HOMO-3 → LUMO, LUMO+1
14	^1E_u	3.636	341	0.999	
15	^1E_u	3.636	341	0.999	

[a]Only spin-allowed transitions with oscillator strength $f > 0$ were selected. For all spin-forbidden $S_0 \rightarrow T_n$ transitions, $f = 0$ due to the absence of the spin−orbital coupling in the used TD-DFT method.

Additionally, we observed a rather weak broad absorption band with the maximum at 409 nm, which was assigned in the literature to a charge-transfer state (CT) of either ligand-to-metal (LMCT) or metal-to-ligand (MLCT) origin.[36] However, our DFT calculations do not support this interpretation. The closest calculated transition with nonzero oscillator strength was found at 3.31 eV and belongs, together with that one at

dx.doi.org/10.1021/jp5036629 | J. Phys. Chem. A 2014, 118, 5419−5426

3.64 eV, to the B band structure of the mostly ligand-centered transitions (HOMO−4, HOMO−3 → LUMO, LUMO+1). All calculated transitions are summarized in the Supporting Information (Tables S1 and S2).

At the lowest concentration $c = 10^{-6}$ M (see Figure 2), the spectrum corresponds to mostly monomeric noninteracting dye molecules. With the increasing concentration of the dye, the main absorption band Q_{00} diminishes and broadens, and the other two bands (Q_{01} and $Q_{01'}$) become less resolved, probably due to the formation of H-aggregates.[36,38,39] Additionally, we observed a very weak absorption band at around 770 nm, which decreased with increasing concentration of the dye. We assigned tentatively this absorption band to the optical transitions in J-aggregates due to its position at longer wavelengths. In order to verify this hypothesis, we investigated changes of this optical band upon addition of a cosolvent (methanol) to the Pc solution in toluene. Methanol is assumed to coordinate to the Pc metal center, preventing thus the aggregate formation.[40,41] Indeed, the optical band assigned to the J-aggregates diminished upon addition of 5 vol % of methanol (see Figure S4 in the Supporting Information). This finding supports the attribution of the optical absorption band at around 770 nm to J-aggregates.[41,42] The addition of methanol also induced an increase of the Q_{00} band. The increase in the optical absorption correlates qualitatively well with the increasing fraction of the monomeric dye molecules due to the aggregates dissociation.

The ground-state geometry of the molecule as obtained by the quantum chemical calculations using the DFT method possesses tetragonal symmetry (D_{4h}, the same as non-substituted NiPc) with inversion. All carbon, nitrogen, and nickel nuclei define a single plane. This structure was verified to be a local minimum by subsequent vibrational frequency calculations showing no imaginary frequency. The all-trans aliphatic substituents are oriented outward from the NiPc macrocycle. Thus, they influence its conformation only slightly by prolongation of the C−C bonds between substituted carbon atoms. This distortion is much smaller compared to that of the macrocycle with a nonperipheral substitution, which induces out-of-plane deformation.[43] The detailed atomic Cartesian coordinates can be found in the Supporting Information. A drawing of the molecular conformation is depicted in Figure S2 (Supporting Information).

The time evolution of the TA spectrum was measured in the toluene solution of compound **1** at concentration $c = 5 \times 10^{-6}$ M upon the excitation with ultrashort laser pulses centered at 670 nm. The spectra are presented separately for the long- and short-wavelength parts of the probed spectrum in Figures 3 and 4, respectively. The detailed kinetic traces for selected wavelengths are shown in Figure 5.

In the spectral region of the ground-state absorption band Q_{00}, we could observe diminishing negative signal accompanied by a hypsochromic shift of its minimum. This negative signal can be identified as a ground-state bleaching (GSB) because of its overlap with the Q_{00} optical absorption band (see Figure 2). Simultaneously, we observed a growing broad positive signal of the excited-state absorption (ESA) strongly overlapping with the GSB (cf. Figure 3a). Further development in this spectral region displays mostly a simple decay of the excited state into the ground state (cf. Figure 3b).

Similar evolution of the TA spectrum was observed in the region between 440 and 600 nm shown in Figure 4. The first recorded transient spectrum (at 0.51 ps delay) shows an optical

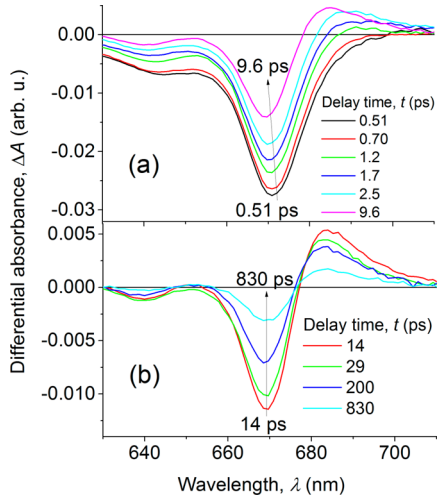

Figure 3. Evolution of TA spectra of the solution of **1** at selected delay times after photoexcitation: (a) short times; (b) longer times.

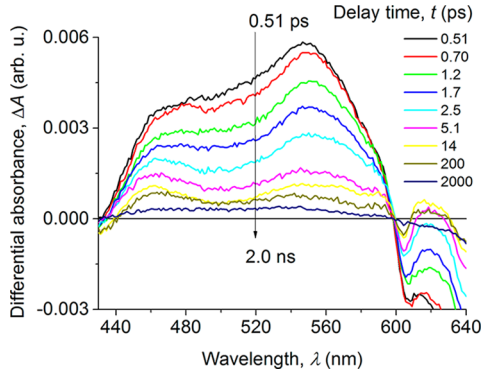

Figure 4. Evolution of the TA spectra observed in solution of the studied compound **1** in the probe wavelength region of 430−640 nm at selected delay times after photoexcitation.

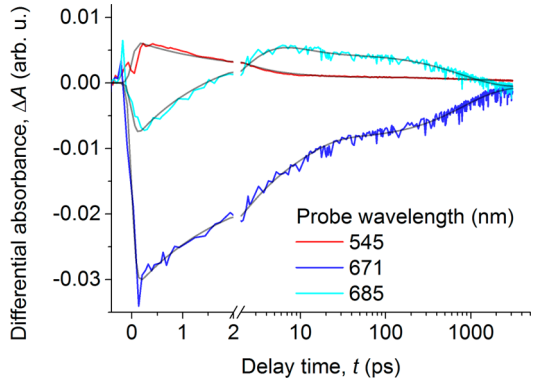

Figure 5. Experimental time traces of TA signals recorded in solution of the studied compound **1** at three representative probe wavelengths (color curves, cf. legend). Also shown are the respective simulated time traces (gray curves) of the proposed kinetic model (see text).

absorption composed of two bands centered at 550 and 460 nm, respectively, the first one being more intense. The longer-wavelength band loses its intensity with a faster rate, so that at t = 5.1 ps after photoexcitation, the intensities of both absorption bands equalize.

More detailed comparison of the kinetic traces is seen in Figure 5. It correlates the development of the TA signals at

dx.doi.org/10.1021/jp5036629 | J. Phys. Chem. A 2014, 118, 5419−5426

probe wavelengths of 545, 685 (ESA bands), and 671 nm (GSB). The experimental time traces of the TA signal recorded at 545 and 685 nm cross each other at the delay time of 2.5 ps. The decay of the former signal correlates well with the increase of the latter one, which reached its maximum at about 7.5 ps. This suggests an ultrafast transition of the excited state into one or several lower-lying states. The early decay of the TA signal at 671 nm probably does not correspond to the excited-state deactivation; rather, it originates in the changes in the ESA band centered at around 685 nm, which strongly overlaps with the GSB signal. As these two contributions have opposite signs, the resulting TA signal was reduced, and the position of its negative peak shifted toward a shorter wavelength (see Figure 3a). Further development of the TA signal at 671 nm (Figure 5) shows a plateau that extends up to about 200 ps when declination of the TA signal strength indicates excited-state deactivation.

Kinetic Model of the Excited-State Evolution. In order to gain insight into the transformations of the excited state, we used a global and target analysis of the TA data. With the help of the global analysis, we deduced the existence of at least four spectrally distinguishable excited states in the relaxation pathway of the photoexcited solution of **1**. In an attempt to identify the contributions of the states found by the DFT calculation (see Table 1) to the observed spectrotemporal TA data $\Delta A(t,\lambda)$, we turned to the target analysis method.[15] It allows one to obtain so-called species-associated differential spectra (SADS)[15,44] $\varepsilon_i(\lambda)$ and evolutions of their concentrations $c_i(t)$ through the separation of the TA data into a number of components i

$$\Delta A(t, \lambda) = \sum_i c_i(t)\varepsilon_i(\lambda) \tag{2}$$

where t is the delay time between the pump and probe pulses and λ is the probe wavelength.

At first, we tried to apply a simple unbranched unidirectional (sequential) four-compartment model, in which the first state is pumped by the photoexcitation and each subsequent state is populated at the expense of a monoexponential decay of the nearest preceding state with no losses involved, while the fourth excited state decays to the ground state. The kinetic equations as well as the resulting set of four SADS together with corresponding concentration evolutions (eq S1 and Figure S3) are given in the Supporting Information. Interestingly, the spectral profiles of the first state with the shortest lifetime and the last longest-living state were very similar in shape. Because a reverse process leading to the recovery of the first state would be thermodynamically unfavorable, we can assume that these two states are created simultaneously upon photoexcitation and that they evolve independently. When comparing the magnitudes of the SADS in the GSB region at around 670 nm, the last SADS was 24 times weaker than the first one, giving the estimate of the fraction of the long-living states to be about 4% of the total population of the photoexcited states.

On the basis of this hypothesis, we adapted the compartmental model to accommodate two branches in which the excited states evolve independently. It can be described by the following system of kinetic differential equations

$$\begin{aligned}
\frac{\mathrm{d}}{\mathrm{d}t}c_{1\mathrm{b}} &= \varphi_{1\mathrm{b}} j_{\mathrm{p}}(t) - \frac{c_{1\mathrm{b}}}{\tau_{1\mathrm{b}}} \\
\frac{\mathrm{d}}{\mathrm{d}t}c_1 &= (1 - \varphi_{1\mathrm{b}}) j_{\mathrm{p}}(t) - \frac{c_1}{\tau_1} \\
\frac{\mathrm{d}}{\mathrm{d}t}c_2 &= \frac{c_1}{\tau_2} - \frac{c_2}{\tau_2} \\
\frac{\mathrm{d}}{\mathrm{d}t}c_3 &= \frac{c_2}{\tau_2} - \frac{c_3}{\tau_3}
\end{aligned} \tag{3}$$

Here, t denotes the time. The term $j_{\mathrm{p}}(t) = \exp(-t^2/2\tau_{\mathrm{p}}^2)$ represents the approximation of the temporal instrument response function (IRF), mainly governed by the time envelope of the pump pulse. The time constants τ_{p} as well as the lifetimes τ_i, $i \in \{1, 2, 3\}$, and $\tau_{1\mathrm{b}}$ were taken as parameters optimized using TIMP software algorithms. The subscript 1b indicates the parameter of the independent parallel branch of the long-living excited states. The value of the branching weight factor $\varphi_{1\mathrm{b}}$ = 0.04 corresponding to the quantum yield of the long-living states was deduced from the intensities of the SADS obtained by fitting the previous model (vide supra).

The lifetime parameters calculated according to the model (see eq 3) are summarized in Table 1. They were found by optimization of the model for the whole set of experimental spectral channels (in the wavelength range of 420−800 nm), which allowed us to obtain a set of SADS characterized by $\varepsilon_i(\lambda)$ and time-dependent concentrations $c_i(t)$ (see Figure 6). The kinetics calculated according to the model reconstruct well the experimental time traces (see the gray curves in Figure 5).

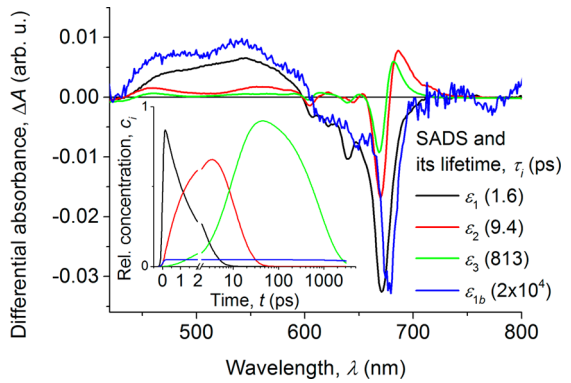

Figure 6. SADS $\varepsilon_i(\lambda)$ and evolution of the excited-state concentrations $c_i(t)$ (inset) relative to the initially photoexcited state obtained by fitting the experimental data using the proposed model. Corresponding lifetimes are shown in parentheses.

By DFT calculations, we found the ground state S_0 to be of $^1A_{1g}$ symmetry, in accordance with the literature.[36] Additionally, below the optically accessible first singlet excited double-degenerate state with symmetry ^1E_u, we have found a number of excited states with triplet multiplicity (see Table 1). The metallic d orbitals of the central Ni atom in **1** induce a strong spin−orbit coupling, which should assist the ultrafast ISC from the photoexcited singlet state S_1 to the triplet manifold, similarly as was reported for other Pc's[3] and porphyrin compounds.[45] A potential candidate to accept the population of the decaying S_1 (with ^1E_u symmetry) would be the energetically close-lying triplet state with symmetry $^3A_{2g}$. Although the calculations suggest that the $^3A_{2g}$ state has a

dx.doi.org/10.1021/jp5036629 | J. Phys. Chem. A 2014, 118, 5419−5426

174 meV higher vertical transition energy from the S_0 than S_1 (^1E_u), its relaxed minimum could still be below that of S_1, possibly due to the spin−orbit interaction or specific interactions with molecules of the solvent, which are not considered in the model. According to our time-resolved spectroscopic observations and modeling, the $^3A_{2g}$ excited state has the lifetime $\tau_1 = (1.60 \pm 0.04)$ ps, exhibits respective SADS $\varepsilon_1(\lambda)$, and follows population kinetics of $c_1(t)$ (cf. Figure 6). According to this hypothesis, the TA spectrum of the directly photoexcited S_1 state was not experimentally accessible due to the ultrafast ISC (the estimated lifetime of S_1 is <100 fs).

The subsequent deactivation pathway would proceed through the population of the lower-lying triplet states, namely, the pair of doubly degenerate states with the ^3E_u and ^3E_g symmetries, as well as the nondegenerate $^3B_{1g}$ state, which were found to be energetically well separated from the state $^3A_{2g}$. We can assign the concentrations $c_2(t)$ and $c_3(t)$ with their respective lifetimes $\tau_2 = (9.4 \pm 0.5)$ ps and $\tau_3 = (814 \pm 25)$ ps to these states. Because the spectral profiles of the respective SADS $\varepsilon_2(\lambda)$ and $\varepsilon_3(\lambda)$ are not very different, it may be possible that both belong to the same symmetry (either ^3E_u or ^3E_g), in which the degeneracy was broken by some interaction. Also, some of the states may not be active in the excited-state pathway. A convincing one-to-one identification remains elusive.

Finally, we will discuss the quantum chemical nature of the excited state with SADS profile $\varepsilon_{1b}(\lambda)$ (cf. Figure 6) and the longest observed lifetime (τ_{1b} > 20 ns; only lower limit obtained due to the limited delay line of our experimental setup). Its spectral shape $\varepsilon_{1b}(\lambda)$ is similar to the $\varepsilon_1(\lambda)$ in both the ESA (430−600 nm) and GSB regions (600−730 nm); the $\varepsilon_{1b}(\lambda)$ contains somewhat more noise (due to low TA intensity in longer delays), and its GSB signal shows a bathochromic shift of about 7 nm, which affects also its vibrational progression peaks.

The bathochromic shift of the GSB signal brought us to the hypothesis that the long-living states originate in J-aggregates. We assume that these J-aggregates could be formed even at the low concentration used in our TA experiment as a result of specific interactions with solvent molecules, which may disturb the cofacial arrangement of H-aggregates preferred at higher concentration[3,36] (vide supra); in other words, we assume a dynamic equilibrium between the monomeric form and various types of aggregates established for the given dye concentration. When analyzing our TA experimental data, we assume various aggregation configurations to be static within the period of the scanned delay time. In the spectral shape $\varepsilon_{1b}(\lambda)$, we can also find the negative peak at around 770 nm, which does not appear in the $\varepsilon_1(\lambda)$. It spectrally coincides with the weak absorption band found in the low-concentration solutions of the studied compound **1**, which we also attribute to the transition in J-aggregates (cf. Figure 2). That also led us to the identification of the long-living excited states with J-aggregates in solution. The presumed J-aggregation breaks the D_{4h} symmetry observed in the isolated molecules (monomers), and thus, it breaks also the degeneration of the first two transitions from the ground state S_0 singlet states S_1 listed in Table 1 for monomers. Then, the negative peaks observed at 677 and 770 nm in the spectral shape $\varepsilon_{1b}(\lambda)$ and in the linear absorption spectrum (see Figure 2) would belong to the transitions $S^J_0 \rightarrow S^J_2$ and $S^J_0 \rightarrow S^J_1$, respectively.

The singlet oxygen photogeneration quantum yield was measured by us to verify the triplet nature of the long-living photoexcited states. It is known from the literature that the Pc, in general, can serve as a photosensitizer of the photocatalytic production of singlet oxygen (metastable state $a^1\Delta_g$).[46,47] The process is controlled by diffusion and collisions between oxygen molecules in the triplet ground state ($X^3\Sigma_g^-$) and the photosensitizer in the triplet excited state. Its quantum yield φ_Δ strongly depends on the quantum yield and lifetime of the triplet state of the photosensitizer. The energy-transfer rate from the Pc molecule to oxygen in toluene stored in an ambient atmosphere was reported[48] to be about $k_{ET} = 3 \times 10^6$ s^{-1}. This value was measured for another Pc derivative, in which the lifetime of the photoexcited triplet state was controlled almost exclusively by collisions with oxygen molecules dissolved in toluene. Therefore, it can give us an estimate of the time scale of the intermolecular energy transfer if we neglect the differences in the spin statistics and energy overlaps between the Pc reported in ref 48 and the compound **1** in our present work.

We measured the quantum yield of the singlet oxygen production in toluene solution as $\varphi_\Delta = 0.03$. This confirms that the long-living species found by the TA experiment are indeed of triplet spin multiplicity; otherwise, they would not convert molecular oxygen into the singlet form. From the relation $\tau_{1b} = (1/k_{ET})[\varphi_\Delta/(\varphi_{1b} - \varphi_\Delta)]$, we can estimate that the lifetime of the long-living triplet states may be as long as $\tau_{1b} \approx 1$ μs. Moreover, the similarity of the SADS spectral features $\varepsilon_1(\lambda)$ and $\varepsilon_{1b}(\lambda)$ (cf. Figure 6) supports our hypothesis that the first short-lived excited state is also of triplet spin multiplicity.

The energy difference between the singlet state $a^1\Delta_g$ and the ground state $X^3\Sigma_g^-$ of oxygen gives rise to the optical absorption at a photon energy of 0.97 eV.[49] In compound **1**, the lowest triplet state with sufficient energy is the state with symmetry $^3A_{2g}$ calculated at the energy level of 2.086 eV (cf. Table 1). Because we have not studied the aggregation of compound **1** by quantum mechanical calculations, we can only assume that the long-living state originates from a coupling among the triplet states $^3A_{2g}$ found in each of the interacting aggregated monomers.

CONCLUSION

We proposed and gave supporting evidence for the following scenario of the rapid nonradiative deactivation of the photoexcited state S_1 of the peripherally substituted 2,3,9,10,16,17,23,24-octabutoxy nickel(II) phthalocyanine in toluene solution.

On the basis of the results of the global and target analyses of the transient optical absorption spectra, we identified four spectrally distinguishable excited states and constructed the kinetic model based on the evolution of two independent branches. According to our hypothesis, the branching is caused by J-aggregation of the studied material. We could assign the photoexcitation quantum yield of 96% to the monomers and that of 4% to the J-aggregates.

In monomers, the S_1 state (doubly degenerate, with ^1E_u symmetry) undergoes ultrafast ISC with a time scale below the resolution of our experiment. The first observed transient was identified as a triplet state (with symmetry $^3A_{2g}$) that is energetically in close proximity to S_1. Subsequently, this state decays with the lifetime of 1.60 ps through a pathway formed by some of the lower-lying excited triplet states of the ^3E_u, ^3E_g, and $^3B_{1g}$ symmetries. In our model, we found that their effective lifetimes in the kinetic model are 9.4 and 814 ps, respectively; the latter refers to the direct decay into the ground state of $^1A_{1g}$

dx.doi.org/10.1021/jp5036629 | J. Phys. Chem. A 2014, 118, 5419−5426

symmetry. The SADS of these excited states show a strong overlap between the excited-state and the ground-state absorption.

In the case of monomers of NiPc, the major observed effect of the symmetric octabutoxy peripheral substitution is about a 3-fold increase in the lifetime of the excited triplet state, which decays directly to the ground state. In a nonsubstituted analogue, the longest lifetime was reported to be 300 ps, and it was attributed to the excited state of 1^3B_{1g} symmetry.[4] In the case of nonperipheral substitution, the longest lifetime of 640 ps belongs to the excited state with symmetry 1^3A_2. From this comparison, it is apparent, that in the latter case, the effects of electron donation from butoxy substituents and their steric deformation of planarity of the Pc macrocycle partially compensate for each other, yielding only a moderately increased overall lifetime of the excited state.

The excited state in the second branch shows a long lifetime (estimated to be >20 ns). Its SADS profile is similar to that of the short-living state attributed to the state with symmetry $^3A_{2g}$ in monomers but shows a bathochromic shift in the GSB region. This shift supports the identification of the long-living states with the J-aggregates of the studied molecules. With help of the experimental determination of the quantum yield of the singlet oxygen production, we proved their triplet spin multiplicity.

■ ASSOCIATED CONTENT

Ⓢ Supporting Information

Tables listing all of the calculated singlet and triplet absorption transitions of the studied phthalocyanine derivative in toluene; drawing and Cartesian coordinates of the molecular conformation of the studied compound **1** optimized by the DFT method; sequential unbranched evolution model description and its analysis; and dependence of the optical absorption spectrum on the solvent composition. This material is available free of charge via the Internet at http://pubs.acs.org.

■ AUTHOR INFORMATION

Corresponding Author

*E-mail: pfleger@imc.cas.cz. Tel: (+420)296809571. Fax: (+420)296809410.

Author Contributions

The manuscript was written through contributions of all authors. All authors have given approval to the final version of the manuscript.

Notes

The authors declare no competing financial interest.

■ ACKNOWLEDGMENTS

This work was funded by the Technology Agency of the Czech Republic (Id: TE01020022) and by the Ministry of Industry and Trade of the Czech Republic (Id: FR-TI1/144). Travel expenses were supported by the Academy of Sciences of the Czech Republic (Project Id: M200501204) and by the Ministry of Education, Youth and Sports of the Czech Republic (Project Id: KONTAKT LH II 12186). The access to the CERIT-SC computing and storage facilities provided under the program Center CERIT Scientific Cloud, part of the Operational Program Research and Development for Innovations (Project Id: CZ. 1.05/3.2.00/08.0144), is acknowledged.

■ ABBREVIATIONS

DFT, density functional theory; ESA, excited-state absorption; ISC, intersystem crossing; GSB, ground-state bleaching; LMCT, ligand-to-metal charge transfer; MLCT, metal-to-ligand charge transfer; NiPc, nickel phthalocyanine; NiPc(α-O-Bu)$_8$, nonperipherally octabutoxy-substituted nickel phthalocyanine; Pc, phthalocyanine; PCM, polarizable continuum model; SADS, species-associated differential spectra; TA, transient absorption; TD-DFT, time-dependent version of the DFT

■ REFERENCES

(1) Moser, F. H. In *The Phthalocyanines*.; Thomas, A. L., Ed.; CRC Press, Inc.: Boca Raton, FL, 1983; Vol. *II*, Manufacture and Applications.

(2) Ehrler, O. T.; Ji-Ping, Y.; Sugiharto, A. B.; Unterreiner, A. N.; Kappes, M. M. Excited State Dynamics of Metastable Phthalocyanine-Tetrasulfonate Tetra-Anions Probed by Pump/Probe Photoelectron Spectroscopy. *J. Chem. Phys.* **2007**, *127*, 184301.

(3) Nikolaitchik, A. V.; Rodgers, M. A. J. Crown Ether Substituted Monomeric and Cofacial Dimeric Metallophthalocyanines. 2. Photophysical Studies of the Cobalt(II) and Nickel(II) Variants. *J. Phys. Chem. A* **1999**, *103*, 7597−7605.

(4) Soldatova, A.; Kim, J.; Peng, X.; Rosa, A.; Ricciardi, G.; Kenney, M.; Rodgers, M. Effects of Benzoannulation and α-Octabutoxy Substitution on the Photophysical Behavior of Nickel Phthalocyanines: A Combined Experimental and DFT/TDDFT Study. *Inorg. Chem.* **2007**, *46*, 2080−2093.

(5) Fournier, M.; Pépin, C.; Houde, D.; Ouellet, R.; van Lier, J. Ultrafast Studies of the Excited-State Dynamics of Copper and Nickel Phthalocyanine Tetrasulfonates: Potential Sensitizers for the Two-Photon Photodynamic Therapy of Tumors. *Photochem. Photobiol. Sci.* **2004**, *3*, 120−126.

(6) Camerin, M.; Rodgers, M.; Kenney, M.; Jori, G. Photothermal Sensitisation: Evidence for the Lack of Oxygen Effect on the Photosensitising Activity. *Photochem. Photobiol. Sci.* **2005**, *4*, 251−253.

(7) Cuomo, V.; Jori, G.; Rihter, B.; Kenney, M.; Rodgers, M. Tumour-Localising and -Photosensitizing Properties of Liposome-Delivered Ge(IV)-Octabutoxy-Phthalocyanine. *Br. J. Cancer* **1991**, *64*, 93−95.

(8) Millard, R.; Greene, B. Direct Determination of Nonradiative Relaxation Rates in Nonfluorescent Metallophthalocyanines. *J. Phys. Chem.* **1985**, *89*, 2976−2978.

(9) Wöhrle, D.; Schmidt, V. Octabutoxyphthalocyanine, a New Electron Donor. *J. Chem. Soc., Dalton Trans.* **1988**, 549−551.

(10) Sauer, T.; Wegner, G. Control of the Discotic to Isotropic Transition in Alkoxy-Substituted Silicondihydroxo-Phthalocyanines by Axial Substituents. *Mol. Cryst. Liq. Cryst.* **1988**, *162*, 97−118.

(11) Van Nostrum, C.; Picken, S.; Schouten, A.-J.; Nolte, R. Synthesis and Supramolecular Chemistry of Novel Liquid Crystalline Crown Ether-Substituted Phthalocyanines: Toward Molecular Wires and Molecular Ionoelectronics. *J. Am. Chem. Soc.* **1995**, *117*, 9957−9965.

(12) Snellenburg, J. J.; Laptenok, S. P.; Seger, R.; Mullen, K. M.; van Stokkum, I. H. Glotaran: A Java-Based Graphical User Interface for the R Package TIMP. *J. Stat. Software* **2012**, *49*, 1−22.

(13) Mullen, K. M.; van Stokkum, I. H. Timp: An R Package for Modeling Multi-Way Spectroscopic Measurements. *J. Stat. Software* **2007**, *18*, 1−46.

(14) Beechem, J. M.; Ameloot, M.; Brand, L. Global and Target Analysis of Complex Decay Phenomena. *Anal. Instrum.* **1985**, *14*, 379−402.

(15) van Stokkum, I. H.; Larsen, D. S.; van Grondelle, R. Global and Target Analysis of Time-Resolved Spectra. *Biochim. Biophys. Acta, Bioenerg.* **2004**, *1657*, 82−104.

(16) Frisch, M. J.; Trucks, G. W.; Schlegel, H. B.; Scuseria, G. E.; Robb, M. A.; Cheeseman, J. R.; Scalmani, G.; Barone, V.; Mennucci,

B.; Petersson, G. A.; et al. *Gaussian 09*, revision C.01; Gaussian, Inc.: Wallingford, CT, 2009.
(17) Zhao, Y.; Truhlar, D. Density Functionals with Broad Applicability in Chemistry. *Acc. Chem. Res.* **2008**, *41*, 157−167.
(18) Ueno, L.; Jayme, C.; Silva, L.; Pereira, E.; De Oliveira, S.; MacHado, A. Photophysics and Spectroscopic Properties of Zinc Phthalocyanine Revisited Using Quantum Chemistry. *J. Braz. Chem. Soc.* **2012**, *23*, 2237−2247.
(19) Lee, S. Influence of Exchange−Correlation Functional in The Calculations of Vertical Excitation Energies of Halogenated Copper Phthalocyanines Using Time-Dependent Density Functional Theory (TD-DFT). *Bull. Korean Chem. Soc.* **2013**, *34*, 2276−2280.
(20) Anbarasan, P. M.; Senthil Kumar, P.; Geetha, M.; Govindan, R.; Manimegalai, S.; Velmurugan, K. Geometries, Electronic Structures and Electronic Absorption Spectra of Silicon Dichloride Substituted Phthalocyanine for Dye Sensitized Solar Cells. *Recent Res. Sci. Technol.* **2010**, *2*, 8−16.
(21) Kratochvílová, I.; Nešpůrek, S.; Šebera, J.; Záliš, S.; Pavelka, M.; Wang, G.; Sworakowski, J. New Organic FET-Like Photoactive Device, Experiments and DFT Modeling. *Eur. Phys. J. E: Soft Matter Biol. Phys.* **2008**, *25*, 299−307.
(22) Toman, P.; Nešpůrek, S.; Yakushi, K. Electronic States and Infrared Spectroscopy of Ni- and Co-Phthalocyanines: Neutral and Oxidized Forms. *J. Porphyrins Phthalocyanines* **2002**, *6*, 556−562.
(23) Záliš, S.; Kratochvílová, I.; Zambova, A.; Mbindyo, J.; Mallouk, T.; Mayer, T. Combined Experimental and Theoretical DFT Study of Molecular Nanowires Negative Differential Resistance and Interaction with Gold Clusters. *Eur. Phys. J. E: Soft Matter Biol. Phys.* **2005**, *18*, 201−206.
(24) Bauernschmitt, R.; Ahlrichs, R. Treatment of Electronic Excitations within the Adiabatic Approximation of Time Dependent Density Functional Theory. *Chem. Phys. Lett.* **1996**, *256*, 454−464.
(25) Casida, M.; Jamorski, C.; Casida, K.; Salahub, D. Molecular Excitation Energies to High-Lying Bound States from Time-Dependent Density-Functional Response Theory: Characterization and Correction of the Time-Dependent Local Density Approximation Ionization Threshold. *J. Chem. Phys.* **1998**, *108*, 4439−4449.
(26) Stratmann, R.; Scuseria, G.; Frisch, M. An Efficient Implementation of Time-Dependent Density-Functional Theory for the Calculation of Excitation Energies of Large Molecules. *J. Chem. Phys.* **1998**, *109*, 8218−8224.
(27) Becke, A. Density-Functional Thermochemistry. III. The Role of Exact Exchange. *J. Chem. Phys.* **1993**, *98*, 5648−5652.
(28) Lee, C.; Yang, W.; Parr, R. Development of the Colle−Salvetti Correlation-Energy Formula into a Functional of The Electron Density. *Phys. Rev. B: Condens. Matter Mater. Phys.* **1988**, *37*, 785−789.
(29) Yanai, T.; Tew, D.; Handy, N. A New Hybrid Exchange−Correlation Functional Using the Coulomb-Attenuating Method (CAM-B3LYP). *Chem. Phys. Lett.* **2004**, *393*, 51−57.
(30) Jacquemin, D.; Perpète, E.; Scuseria, G.; Ciofini, I.; Adamo, C. TD-DFT Performance for the Visible Absorption Spectra of Organic Dyes: Conventional versus Long-Range Hybrids. *J. Chem. Theory Comput.* **2008**, *4*, 123−135.
(31) Tomasi, J.; Mennucci, B.; Cammi, R. Quantum Mechanical Continuum Solvation Models. *Chem. Rev.* **2005**, *105*, 2999−3093.
(32) Černý, J.; Karásková, M.; Rakušan, J.; Nešpůrek, S. Reactive Oxygen Species Produced by Irradiation of Some Phthalocyanine Derivatives. *J. Photochem. Photobiol., A* **2010**, *210*, 82−88.
(33) Olmsted, J.; Akashah, T. Photooxidation of Isobenzofurans. Dual Mechanism Process. *J. Am. Chem. Soc.* **1973**, *95*, 6211−6215.
(34) Ogunsipe, A.; Maree, D.; Nyokong, T. Solvent Effects on the Photochemical and Fluorescence Properties of Zinc Phthalocyanine Derivatives. *J. Mol. Struct.* **2003**, *650*, 131−140.
(35) Pochekaylov, S.; Rais, D.; Nešpůrek, S.; Rakušan, J.; Karásková, M. Optical Properties of Soluble Phthalocyanines. *J. Optoelectron. Adv. Mater.* **2007**, *9*, 479−482.
(36) Stillman, M. J.; Nyokong, T. Absorbtion and Magnetic Circular Dichroism Spectral Properties of Phthalocyanines Part 1: Complexes of the Dianion, Pc(−2). In *Phthalocyanines: Properties and Applications*; Leznoff, C., Lever, A., Eds.; VCH: New York, 1989; pp 138−289.
(37) Schaffer, A.; Gouterman, M.; Davidson, E. Porphyrins XXVIII. Extended Hückel Calculations on Metal Phthalocyanines and Tetrazaporphins. *Theor. Chim. Acta* **1973**, *30*, 9−30.
(38) Yonehara, Y.; Yakushi, K. High-Pressure Study of One-Dimensional Phthalocyanine Conductor, $NiPc(AsF_6)_{0.5}$. *Synth. Met.* **1998**, *94*, 149−155.
(39) Fox, J. M.; Katz, T. J.; Van Elshocht, S.; Verbiest, T.; Kauranen, M.; Persoons, A.; Thongpanchang, T.; Krauss, T.; Brus, L. Synthesis, Self-Assembly, and Nonlinear Optical Properties of Conjugated Helical Metal Phthalocyanine Derivatives. *J. Am. Chem. Soc.* **1999**, *121*, 3453−3459.
(40) Cong, F.; Li, J.; Ma, C.; Gao, J.; Duan, W.; Du, X. Tuning J-Type Dimers of Non-Peripherally Substituted Zinc Tetra-4-tert-butylphenophthalocyanine. *Spectrochim. Acta, Part A* **2008**, *71*, 1397−1401.
(41) Saka, E. T.; Göl, C.; Durmuş, M.; Kantekin, H.; Bıyıklıoğlu, Z. Photophysical, Photochemical and Aggregation Behavior of Novel Peripherally Tetra-Substituted Phthalocyanine Derivatives. *J. Photochem. Photobiol., A* **2012**, *241*, 67−78.
(42) Snow, A. Phthalocyanine Aggregation. In *The Porphyrin Handbook*; Kadish, K. M., Smith, K. M., Guilard, R., Eds.; Academic Press: Amsterdam, The Netherlands, 2003; pp 129−176.
(43) Gunaratne, T.; Gusev, A.; Peng, X.; Rosa, A.; Ricciardi, G.; Baerends, E.; Rizzoli, C.; Kenney, M.; Rodgers, M. Photophysics of Octabutoxy Phthalocyaninato-Ni(II) in Toluene: Ultrafast Experiments and DFT/TDDFT Studies. *J. Phys. Chem. A* **2005**, *109*, 2078−2089.
(44) Ameloot, M.; Beechem, J. M.; Brand, L. Compartmental Modeling of Excited-State Reactions: Identifiability of the Rate Constants from Fluorescence Decay Surfaces. *Chem. Phys. Lett.* **1986**, *129*, 211−219.
(45) Antipas, A.; Gouterman, M. Porphyrins. 44. Electronic States of Cobalt, Nickel, Rhodium, and Palladium Complexes. *J. Am. Chem. Soc.* **1983**, *105*, 4896−4901.
(46) Ishii, K. Functional Singlet Oxygen Generators Based on Phthalocyanines. *Coord. Chem. Rev.* **2012**, *256*, 1556−1568.
(47) Kluson, P.; Drobek, M.; Strasak, T.; Krysa, J.; Karaskova, M.; Rakusan, J. Sulphonated Phthalocyanines as Effective Oxidation Photocatalysts for Visible and UV Light Regions. *J. Mol. Catal. A: Chem.* **2007**, *272*, 213−219.
(48) Ishii, K.; Takeuchi, S.; Shimizu, S.; Kobayashi, N. A Concept for Controlling Singlet Oxygen ($1\Delta g$) Yields Using Nitroxide Radicals: Phthalocyaninatosilicon Covalently Linked to Nitroxide Radicals. *J. Am. Chem. Soc.* **2004**, *126*, 2082−2088.
(49) Ellis, J.; Kneser, H. Kombinationsbeziehungen im Absorptionsspektrum des flüssigen Sauerstoffs. *Z. Phys.* **1933**, *86*, 583−591.